



External auditory canal and middle ear tumors: characterization by morphology and diffusion features on CT and MRI

Peng Wang¹ · Heng Zhang¹ · Jing Zhao¹ · Hongyan Qiao¹ · Yuxi Ge¹ · Qingjun You² · Shudong Hu¹

Received: 19 April 2022 / Accepted: 13 June 2022 / Published online: 17 July 2022
© The Author(s), under exclusive licence to Springer-Verlag GmbH Germany, part of Springer Nature 2022

Abstract

Purpose To explore the value of morphology and diffusion features on CT and MRI in the characterization of external auditory canal and middle ear tumors (EAMETs).

Methods Forty-seven patients with histologically proved EAMETs (23 benign and 24 malignant) who underwent CT and MRI were retrospectively analyzed in this study. CT and MRI characteristics (including size, shape, signal intensity, border, enhancement degree, and bone changes) and apparent diffusion coefficient (ADC) value were analyzed and compared between benign and malignant EAMETs. Logistic regression, receiver operating characteristic (ROC) curve, and Delong test were performed to assess the diagnostic performance.

Results Compared with benign tumors, the malignant EAMETs are characterized by irregular shape, ill-defined border, invasive bone destruction, and intense enhancement (all $p < 0.05$). There were no significant differences on the size and signal intensity between benign and malignant tumors. The ADC value of malignant tumors were $(879.96 \pm 201.15) \times 10^{-6} \text{ mm}^2/\text{s}$, which was significantly lower than benign ones ($p < 0.05$). Logistic regression demonstrates the presence of ill-defined margin, invasive bone destruction, and low ADC value ($\leq 920.33 \times 10^{-6} \text{ mm}^2/\text{s}$) have significant relationship with malignant EAMETs. The combination of characterization by morphology and diffusion features on CT and MRI can further improve the diagnostic efficiency when compared with morphology and diffusion features alone (both $p < 0.05$).

Conclusion Some CT and MRI characteristics are helpful in identifying malignant EAMETs from benign ones (especially ill-defined margin, invasive bone destruction, and low ADC value), and the combination of morphology and diffusion features on CT and MRI has best diagnostic efficiency for discriminating these two entities.

Keywords Temporal bone tumor · External auditory canal · Middle ear · Auricular tumors · Magnetic resonance imaging · Diffusion weighted imaging

Peng Wang, Heng Zhang, and Jing Zhao contributed equally to this study.

✉ Qingjun You
youqingjun@jiangnan.edu.cn

✉ Shudong Hu
hsd2001054@163.com

¹ Department of Radiology, Affiliated Hospital of Jiangnan University, 1000 Hefeng Road, Wuxi 214122, People's Republic of China

² Department of Thoracic Surgery, Affiliated Hospital of Jiangnan University, 1000 Hefeng Road, Wuxi 214122, People's Republic of China

Introduction

The external auditory canal and middle ear contain a wide spectrum of benign and malignant tumors [1]. Since the early signs and symptoms are non-specific, benign and malignant tumors in this area can have similar manifestations [2]. Clinically, patients with malignant external auditory canal and middle ear tumors (EAMETs) often have an overall poor prognosis and generally require radiation therapy and chemotherapy as well as surgical resection [3, 4], whereas patients with benign tumors, such as papilloma, only undergo complete surgical resection [5]. Thus, the differentiation of benign and malignant EAMETs is greatly essential for therapeutic decisions and prognosis.

Temporal bone is irregular and located at the sides and base of the skull, which hinders the physical examination of

the tumors in this area. Hence, imaging techniques, such as CT and MR imaging, play an important role in the diagnosis of auricular tumors. CT is highly sensitive in detecting the osseous invasion, and MRI is superior to CT in the demonstration of early lesions without bony destruction or those with an associated soft tissue component and extraosseous involvement, or the description of the possible invasion into the membranous labyrinth [6, 7]. Thus, imaging approach is important in specifying benign and malignant tumors in this region. Moreover, advanced MRI techniques, such as diffusion-weighted MRI (DWI), have the potential to reflect the physiological and functional information [8]. As previously reported, DWI has been used to discriminate between benign and malignant head and neck lesions [9, 10]. High-resolution DWI using readout-segmented echo-planar imaging (termed RESOLVE) can offer higher signal-to-noise ratio and resolution in the head and neck areas than conventional single shot echo planar image (SS-EPI) DWI [11, 12], thus potentially improving the diagnostic efficiency and reliability of ADC value. Thus, the present study aims to explore morphology and high-resolution diffusion features on CT and MRI to discriminate these two entities.

Materials and methods

Patient selection

Our institutional review board approved this retrospective study, and the requirement for patient informed consent was waived due to the retrospective nature of this study. Seventy consecutive patients with benign and malignant EAMETs were recruited from January 2015 to December 2019. The recruitment based on the following inclusion criteria: (1) all tumors were confirmed by histopathology (surgery/biopsy) and (2) standard CT, MRI, and RESOLVE-DWI were performed. The exclusion criteria were as follows: (1) image quality was insufficient because of severe artifacts ($n=5$); (2) patients had a history of treatment or recurrence before CT, MRI and RESOLVE-DWI examinations ($n=10$); (3) the maximum diameter of the tumors ≤ 1 cm ($n=8$).

CT protocol

The CT examinations were performed on a CT scanner (Somatom Definition; Siemens Healthcare, Erlangen, Germany). The following parameters were used for data acquisition: tube voltage = 120 kVp; tube current = 240 mAs; pitch = 0.8; slice thickness = 2 mm; and field of view (FOV) = 220 × 240 mm. The soft tissue and bone algorithm reconstruction images were automatically obtained with or without intravenous injection of 70 ml iopamidol (320 mg I/ml; Isovue, Bracco Diagnostics, Inc, Singen, Germany).

MRI protocol

All scans were performed on a 3.0 T MR scanner (MAGNETOM, Verio, Siemens, Erlangen, Germany) using a 12-channel head coil. Conventional MRI consisted of an axial fast spin-echo T1-weighted imaging (T1WI) (repetition time [TR] = 384 ms, echo time [TE] = 9.1 ms), an axial fast spin-echo T2-weighted imaging (T2WI) (TR = 4000 ms, TE = 99 ms) with or without fat suppression, and axial, coronal and sagittal contrast-enhanced T1WI with fat suppression. Gadolinium-enhanced three-dimensional gradient recalled-echo T1-weighted imaging (3D-GRE-T1WI) was performed after intravenous injection of 0.1 mmol/kg of Gd-DTPA (Magnevist, Bayer Schering, Berlin, Germany) at a rate of 2 ml/s, followed by 20 ml of 0.9% saline flush using a power injector, with a matrix of 192 × 192, a field of view (FOV) of 220 × 220 mm, and a thickness/gap of 2/0.2 mm. For RESOLVE-DWI, a readout-segmented EPI, parallel imaging and two-dimensional navigator-based reacquisition were used; all DWI sequences were scanned axially. The parameters were as follows: TR = 4700 ms, TE = 66 ms; slice thickness/gap = 2/0.2 mm; matrix = 192 × 192; FOV = 240 × 240 mm; readout segments = 7; number of excitation = 1; gradient factors: $b = 0, 1000$ s/mm²; diffusion directions = 3.

Imaging analysis

Two radiologists (readers 1 and 2), who had 7 and 8 years of experience in head and neck imaging, respectively, were blinded to the patients' histopathology before they independently analyzed the images. Disagreements were resolved through further discussion with a third radiologist (with 20 years of experience) to reach a consensus. The features of the mass, including size, shape, signal intensity, border, enhancement degree, and bone changes, were assessed. The sizes were measured in maximum dimensions on the transverse plane. The shape was defined as round/oval or irregular. Signal intensity was classified as homogeneous or heterogeneous on both pre- and post-contrast CT and MR images. The border of the tumor was described as well-defined (more than two thirds of the border was sharply demarcated) or ill-defined (less than one-third of the border was sharply demarcated). The enhancement degree was described as poor-moderate (similar to or greater than muscles, but lower than blood vessels), or intense (similar to the blood vessels). Bone changes were defined as expansive change or invasive destruction on CT images.

To quantitatively analyze the data acquired from the RESOLVE-DWI, two radiologists blinded to the clinical

and histopathological data measured the ADC values of the tumors by drawing ROIs (mean area, 117.17 mm²; range, 33.12–445.40 mm²) on an offline workstation, taking care to exclude obvious hemorrhagic and necrotic areas and avoid the most peripheral portions to exclude partial volume effects of adjacent extralesional tissue. The measurements made by readers 1 and 2 were averaged for statistical analysis.

Statistical analysis

The demographic, CT and MRI features between benign and malignant EAMETs were compared by using the chi-square test for categorical variables and the *t* test for noncategorical data. If the categorical count data was less than five, Fisher's exact test was applied instead. Then, significant CT and MRI characteristics as well as the ADC value were included into multivariate logistic regression analyses to calculate the odds ratios (ORs) with 95% confidence intervals (CIs). Receiver operating characteristic (ROC) curves were used to evaluate the sensitivity, specificity, positive predictive value (PPV), negative predictive value (NPV), accuracy of RESOLVE-DWI, CT + MRI, and CT + MRI + RESOLVE-DWI. DeLong test was used to compare the AUCs for further assess their diagnostic efficacy [13]. The kappa values and interclass correlation coefficients (ICCs) were calculated to evaluate inter-reader agreement of qualitative and quantitative features on the CT and MRI, respectively. Kappa values of 0.61 to 1.00 indicated substantial to almost perfect agreement [14], and ICC > 0.75 was considered to indicate a good to excellent reliability agreement [15]. The statistical analyses were performed using the MedCalc statistical software (Version 15.2.2, Ostend, Belgium) and SPSS statistical package (Version 22.0, Chicago, IL). A *p*-value < 0.05 was considered to indicate a statistically significant difference.

Results

As summarized in Table 1, a cohort of 47 patients consisting of 23 patients with benign tumors (8 males and 15 females; mean age 47 ± 11 years) and 24 patients with malignant ones (11 males and 13 females; mean age 50 ± 14 years) was included in this study. The shape, border, bone change, and enhancement degree of malignant tumors were all significantly different from those of benign ones (*p* < 0.05). Compared with benign tumors, the malignant EAMETs are characterized by irregular shape, ill-defined border, invasive bone destruction, and intense enhancement (Figs. 1, 2, Table 2). In addition, the size and signal intensity were not significantly different between the benign and malignant tumors (*p* > 0.05).

Malignant EAMETs exhibited significantly lower ADC values than benign entities (*p* < 0.05), and the tumor with an ADC ≤ 920.33 × 10⁻⁶ mm²/s were more likely to be malignant lesions than those with an ADC > 920.33 × 10⁻⁶ mm²/s. Multivariate logistic regression analysis suggested that tumors with ill-defined margin, invasive bone destruction, and low ADC (≤ 920.33 × 10⁻⁶ mm²/s) were more likely to be malignant than those without this finding (OR = 13.06, 95% CI = 5.09–19.10, *p* < 0.001; OR = 2.76, 95% CI = 0.91–5.36, *p* = 0.022; and OR = 16.24, 95% CI = 9.38–31.99, *p* < 0.001, respectively).

As presented in Fig. 3 and Table 3, the ROC curves showed that the AUCs of RESOLVE-DWI, CT + MRI, and CT + MRI + RESOLVE-DWI for differentiating benign and malignant tumors were 0.789, 0.851, and 0.961, respectively. Significant differences of AUC were found between CT + MRI and CT + MRI + RESOLVE-DWI (*Z* = 2.72, *p* < 0.05), and between RESOLVE-DWI and CT + MRI + RESOLVE-DWI (*Z* = 2.398, *p* < 0.05).

As shown in Table 4, the inter-reader agreements were substantial to almost perfect for qualitative features (size, ADC), good to excellent for quantitative parameters on the

Table 1 Demographic and histology of benign and malignant EAMETs

Parameters	Benign tumors (<i>n</i> = 23)	Malignant tumors (<i>n</i> = 24)
Age (years)	47 ± 11	50 ± 14
Gender		
Male	8	11
Female	15	13
Location		
External auditory canal	(1) Papilloma (<i>n</i> = 3)	(1) Squamous cell carcinoma (<i>n</i> = 14) (2) Adenoid cystic carcinoma (<i>n</i> = 2)
Middle ear and mastoid portions	(1) Facial nerve schwannoma (<i>n</i> = 17) (2) Glomus tympanicum tumor (<i>n</i> = 3)	(1) Squamous cell carcinoma (<i>n</i> = 7) (2) Metastasis (<i>n</i> = 1)



Fig. 1 Facial nerve schwannoma in a 35-year-old man. Axial CT soft tissue image (A) and bone algorithm reconstruction image (B) shows that a mass predominantly locates in the right middle ear and mastoid portions with expansive bone change. Axial T2W (C) and T1W (D) imaging demonstrate an oval, well-defined homogeneous

signal lesion with compressive bone resorption. A post-contrast axial T1W image (E) and coronal T1W image (F) reveal a mild enhanced mass. The mass showed hypointensity on the RESOLVE-DWI (G). On the ADC map (H), the mass showed a high signal intensity with an ADC value of $974.17 \times 10^{-6} \text{ mm}^2/\text{s}$

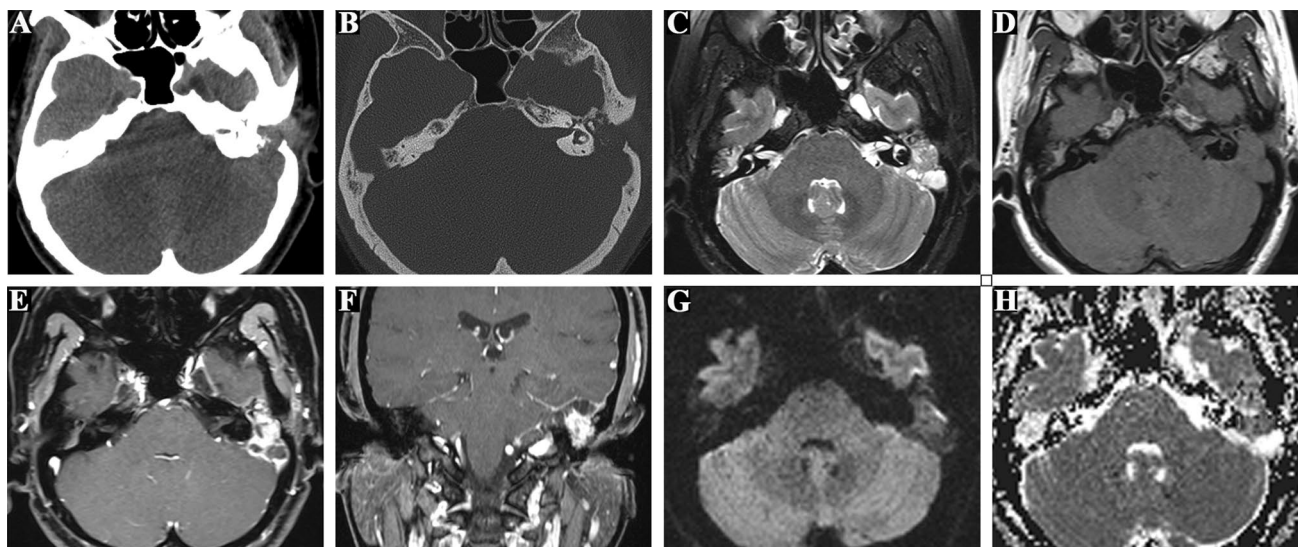


Fig. 2 Squamous cell carcinoma in a 57-year-old man. Axial CT soft tissue image (A) and bone algorithm reconstruction image (B) shows that a mass predominantly locates in the left middle ear and mastoid portions with invasive bone destruction. Axial T2W (C) and T1W (D) imaging demonstrate an irregular, ill-defined heterogeneous sig-

nal lesion with invasive bone destruction. A post-contrast axial T1W image (E) and coronal T1W image (F) reveal an intense enhanced mass. The mass showed hyperintensity on the RESOLVE-DWI (G). On the ADC map (H), the mass showed a low signal intensity with an ADC value of $706.27 \times 10^{-6} \text{ mm}^2/\text{s}$

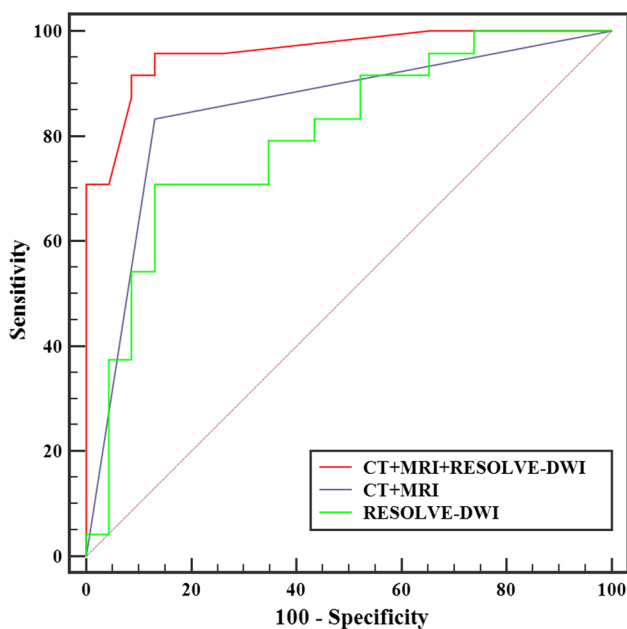
CT and MRI (shape, signal intensity, border, enhancement degree, and bone changes).

Discussion

The incidence of EAMETs is low, and its signs and symptoms are non-specific [2, 3]. Hence, malignant tumors are often misdiagnosed as benign diseases with similar

Table 2 The CT and MRI features of benign and malignant EAMETs

Features	Benign tumors (n=23)	Malignant tumors (n=24)	<i>p</i> value
Size (cm)	1.91 ± 0.90	2.41 ± 1.08	0.100
Shape			0.006
Round/oval	15	6	
Irregular	8	18	
Border			<0.001
Well-defined	20	5	
Ill-defined	3	19	
Bone changes			<0.001
Expansive	20	6	
Invasive	3	18	
Signal intensity			0.680
Homogeneous	8	7	
Heterogeneous	15	17	
Enhancement degree			0.036
Mild–moderate	9	3	
Intense	14	21	
ADC ($\times 10^{-6}$ mm ² /s)	1157.95 ± 318.74	879.96 ± 201.15	0.001

**Fig. 3** ROC curves of RESOLVE-DWI, CT+MRI, and CT+MRI+RESOLVE-DWI for differentiating benign and malignant EAMETs

symptoms, and the treatment is delayed. The morphologic and diffusions characteristics can offer better characterization their anatomic relationship with surrounding structures and physiological processes. Therefore, the imaging technologies are of great significance in the differential

diagnosis of benign and malignant EAMETs, contributing to select optimal treatment strategies and improve prognosis of patients. In this study, the presence of ill-defined border, invasive bone destruction, and $ADC \leq 920.33 \times 10^{-6}$ mm²/s were the most valuable CT and MRI features that may be helpful for differentiating these two entities. With a combination of the morphologic and diffusions characteristics on CT and MRI, optimal sensitivity, specificity, and accuracy was achieved in the discrimination of benign and malignant EAMETs.

Malignant EAMETs typically show aggressive manner, while benign tumors, such as facial nerve schwannoma, often present as an enlargement of the bony delineation and well-defined sharp margin [16, 17]. In this study, the CT and MRI morphological characteristics of margin, and bone change were significantly different between benign and malignant EAMETs, and the lesion with ill-defined margin and invasive bone destruction was more likely to be malignant EAMETs than those without these findings. This finding was consistent with a previous study in head and neck lesions [7, 18, 19]. In addition, no previous studies have compared the enhancement degrees of benign and malignant EAMETs on CT and MRI. In our study, benign tumors showed less intense enhancement than malignant ones. This finding might be explained by increased neovascularization in malignancies, which may play a key role in supplying nutrition for the development and metastasis [20]. But it should be noted that some benign tumor of auricular area, such as glomus tympanicum tumor, may also demonstrate intense enhancement similar to malignancies [21, 22]; thus, comprehensive evaluation of the radiological features on CT and MRI is still important in clinical practice. In addition, our study found benign tumors are of regular shape (such as round or oval shape) but malignant tumor is of irregular shape. However, some benign tumors, such as facial nerve schwannoma, can also exhibit a lytic lesion when they centered on the geniculate ganglion, leading to these benign tumors with an irregular shape [23]. In our study, the signal intensity finding was not sufficiently specific for the differentiation of benign and malignant EAMETs. This may be due to some benign tumors, such as schwannoma, can have intratumoral cystic change and subacute hemorrhage [24]. However, these findings cannot be ignored when diagnosing a lesion involving this area. For example, malignant tumors, such as squamous cell carcinoma commonly appear as heterogeneous lesions on MRI [23].

Diffusion-weighted imaging (DWI) can quantitatively reflect the random motion of water molecules in biological tissues, contributing to noninvasively reflecting cellularity within lesions using the apparent diffusion coefficient (ADC) value [25]. However, the conventional single-shot echo-planar imaging (SS-EPI) DWI is prone to generate susceptibility distortion due to the air-bone interface of the

Table 3 Diagnostic performance of RESOLVE-DWI, CT + MRI and CT + MRI + RESOLVE-DWI in the differentiation between benign and malignant tumors

	Cut-off value	AUC (95% CI)	Sen (%) (95% CI)	Spe (%) (95% CI)	PPV (%) (95% CI)	NPV (%) (95% CI)	Acc (%) (95% CI)
Resolve-DWI	0.920	0.789 (0.645–0.894)	70.83 (48.90–87.40)	86.96 (66.40–97.20)	85.00 (62.10–96.80)	74.10 (53.70–88.90)	79.06 (57.84–92.40)
CT + MRI	0.166	0.851 (0.717–0.938)	83.33 (62.60–95.30)	86.96 (66.40–97.20)	87.00 (66.40–97.20)	83.30 (62.60–95.30)	85.75 (64.54–96.27)
CT + MRI + RESOLVE-DWI	0.431	0.961* (0.860–0.996)	91.67 (73.00–99.00)	91.30 (72.00–98.90)	91.70 (73.00–99.00)	91.30 (72.00–98.90)	91.42 (72.48–98.95)

AUC area under the curve; Sen sensitivity; Spe specificity; NPV negative predictive value; PPV positive predictive value; Acc accuracy; CI confidence intervals

*The AUC values of CT + MRI + RESOLVE-DWI were significantly higher than those of CT + MRI and RESOLVE-DWI (both $p < 0.05$)

Table 4 Inter-reader agreement for qualitative features and quantitative parameters on the CT and MRI

	ICC (95% CI)	Kappa value (95% CI)
Size	0.898 (0.854–0.949)	–
Shape	–	0.872 (0.817–0.924)
Border	–	0.820 (0.759–0.873)
Bone changes	–	0.831 (0.756–0.873)
Signal intensity	–	0.849 (0.803–0.883)
Enhancement degree	–	0.854 (0.786–0.902)
ADC ($\times 10^{-6}$ mm ² /s)	0.879 (0.826–0.935)	–

ICC intraclass correlation coefficient; CI confidence interval

auricular region [26, 27]. The newly developed RESOLVE-DWI approach significantly improves image quality by reducing the susceptibility artifacts, distortion and blurring when compared with SS-EPI [28]. Thus, RESOLVE-DWI can offer more accurate ADC values than SS-EPI for auricular tumors. In this study, we found that the mean ADC value of malignant EAMETs was significantly lower than that of the benign entities. This finding was in accordance with previous study by Yu et al., who found significantly lower ADC value in malignant tumor than that of benign lesion [29]. These may be due to high cellularity in malignancies, which can effectively restrict the water molecule diffusion of tumors, resulting in significantly low ADC values [30, 31]. In the present study, the threshold value of 920.33×10^{-6} mm²/s for ADC provided a relative high sensitivity, specificity, and accuracy for differentiating these two entities. Hence, our study revealed that ADC could be a useful imaging parameter for the differentiation of benign and malignant EAMETs. Furthermore, our results found that the combination of the morphologic and diffusions characteristics on CT and MRI can obtain the significant higher accuracy than the morphologic and diffusions characteristics alone in the differentiation of benign and malignant tumors, indicating that the comprehensive analysis of morphologic and diffusions characteristics may be the optimal approach for discriminating malignant tumors of external auditory canal and middle ear from benign ones.

The present study has several limitations. First, the retrospective study harbored potential bias. Second, the measurement of ADC value did not correlate with histological findings on a site-to-site basis. Thus, further studies are needed to investigate the findings of these correlations. Third, given the wide variety of histologic types of benign and malignant tumors, detailed subgroup analyses of the conventional CT, MRI findings and ADC values should be performed in future.

In conclusion, some CT and MRI characteristics are helpful in identifying malignant EAMETs from benign ones (especially ill-defined margin, invasive bone destruction, and low ADC value), and the combination of morphology and diffusion features on CT and MRI have best diagnostic efficiency for discriminating these two entities, which could be highly valuable for earlier therapy and improving the prognosis for patients with EAMETs.

Funding This study was supported by a grant-in-aid for scientific research from the Technology Plan of Jiangsu (No. H2019087), Translational Medicine Project of Wuxi health commission (No. ZZ002), and Youth Project of Wuxi health commission (No. Q202112).

Declarations

Conflict of interest None.

References

1. Juliano AF, Ginat DT, Moonis G (2013) Imaging review of the temporal bone: part I. Anatomy and inflammatory and neoplastic processes. *Radiology* 269(1):17–33. <https://doi.org/10.1148/radiol.13120733>
2. Lionello M, Stritoni P, Facciolo MC et al (2014) Temporal bone carcinoma. Current diagnostic, therapeutic, and prognostic concepts. *J Surg Oncol* 110(4):383–392. <https://doi.org/10.1002/jso.23660>
3. Da Silva AP, Breda E, Monteiro E (2016) Malignant tumors of the temporal bone—our experience. *Braz J Otorhinolaryngol* 82(4):479–483. <https://doi.org/10.1016/j.bjorl.2015.09.010>

4. Prasad SC, D’Orazio F, Medina M et al (2014) State of the art in temporal bone malignancies. *Curr Opin Otolaryngol* 22(2):154–165. <https://doi.org/10.1097/MOO.0000000000000035>
5. McClellan JH, Ewing E, Gupta S (2018) Squamous papilloma of the external auditory canal. *Otol Neurotol* 39(5):e413–e415. <https://doi.org/10.1097/MAO.0000000000001783>
6. Colas L, Caron S, Cotten A (2015) Skull vault lesions: a review. *AJR Am J Roentgenol* 205(4):840–847. <https://doi.org/10.2214/AJR.14.13415>
7. Tu Z, Xiao Z, Zheng Y et al (2019) Benign and malignant skull-involved lesions: discriminative value of conventional CT and MRI combined with diffusion-weighted MRI. *Acta Radiol* 60(7):880–886. <https://doi.org/10.1177/0284185118773541>
8. Wang J, Takashima S, Takayama F et al (2001) Head and neck lesions: characterization with diffusion-weighted echo-planar MR imaging. *Radiology* 220(3):621–630. <https://doi.org/10.1148/radiol.2202010063>
9. Serifoglu I, Oz II, Damar M et al (2015) Diffusion-weighted imaging in the head and neck region: usefulness of apparent diffusion coefficient values for characterization of lesions. *Diagn Interv Radiol* 21(3):208–214. <https://doi.org/10.5152/dir.2014.14279>
10. Bhatt N, Gupta N, Soni N et al (2017) Role of diffusion-weighted imaging in head and neck lesions: Pictorial review. *Neuroradiol J* 30(4):356–369. <https://doi.org/10.1177/1971400917708582>
11. Koyasu S, Iima M, Umeoka S et al (2014) The clinical utility of reduced-distortion readout-segmented echo-planar imaging in the head and neck region: initial experience. *Eur Radiol* 24(12):3088–3096. <https://doi.org/10.1007/s00330-014-3369-5>
12. Holdsworth SJ, Skare S, Newbould RD et al (2008) Readout-segmented EPI for rapid high resolution diffusion imaging at 3 T. *Eur J Radiol* 65(1):36–46. <https://doi.org/10.1016/j.ejrad.2007.09.016>
13. DeLong ER, DeLong DM, Clarke-Pearson DL (1988) Comparing the areas under two or more correlated receiver operating characteristic curves: a nonparametric approach. *Biometrics* 44(3):837–845
14. Landis JR, Koch GG (1977) The measurement of observer agreement for categorical data. *Biometrics* 33(1):159–174
15. Koo TK, Li MY (2016) A guideline of selecting and reporting intraclass correlation coefficients for reliability research. *J Chiropr Med* 15(2):155–163
16. Bird CR, Hasso AN, Stewart CE et al (1983) Malignant primary neoplasms of the ear and temporal bone studied by high-resolution computed tomography. *Radiology* 149(1):171–174. <https://doi.org/10.1148/radiology.149.1.6310679>
17. Wiggins RR, Harnsberger HR, Salzman KL et al (2006) The many faces of facial nerve schwannoma. *AJNR Am J Neuroradiol* 27(3):694–699
18. Garfinkle J, Melancon D, Cortes M et al (2011) Imaging pattern of calvarial lesions in adults. *Skeletal Radiol* 40(10):1261–1273. <https://doi.org/10.1007/s00256-010-0971-8>
19. Yuan Y, Tang W, Tao X (2016) Parotid gland lesions: separate and combined diagnostic value of conventional MRI, diffusion-weighted imaging and dynamic contrast-enhanced MRI. *Br J Radiol* 89(1060):20150912. <https://doi.org/10.1259/bjr.20150912>
20. Marioni G, Nucci R, Marino F et al (2012) Neoangiogenesis in temporal bone carcinoma: the prognostic role of CD105. *Otol Neurotol* 33(5):843–848. <https://doi.org/10.1097/MAO.0b013e318254edc9>
21. Caldemeyer KS, Mathews VP, Azzarelli B et al (1997) The jugular foramen: a review of anatomy, masses, and imaging characteristics. *Radiographics* 17(5):1123–1139. <https://doi.org/10.1148/radiographics.17.5.9308106>
22. Rao AB, Koeller KK, Adair CF (1999) From the archives of the AFIP. Paragangliomas of the head and neck: radiologic-pathologic correlation. *Armed Forces Institute of Pathology. Radiographics* 19(6):1605–1632. <https://doi.org/10.1148/radiographics.19.6.g99no251605>
23. De Foer B, Kenis C, Vercruyse J et al (2009) Imaging of temporal bone tumors. *Neuroimag Clin N Am* 19(3):339–366. <https://doi.org/10.1016/j.nic.2009.06.003>
24. Mundada P, Purohit BS, Kumar TS et al (2016) Imaging of facial nerve schwannomas: diagnostic pearls and potential pitfalls. *Diagn Interv Radiol* 22(1):40–46. <https://doi.org/10.5152/dir.2015.15060>
25. Le Bihan D (1995) Molecular diffusion, tissue microdynamics and microstructure. *NMR Biomed* 8(7–8):375–386. <https://doi.org/10.1002/nbm.1940080711>
26. De Foer B, Vercruyse J, Spaepen M et al (2010) Diffusion-weighted magnetic resonance imaging of the temporal bone. *Neuroradiology* 52(9):785–807. <https://doi.org/10.1007/s00234-010-0742-1>
27. De Foer B, Vercruyse JP, Pilet B et al (2006) Single-shot, turbo spin-echo, diffusion-weighted imaging versus spin-echo-planar, diffusion-weighted imaging in the detection of acquired middle ear cholesteatoma. *AJNR Am J Neuroradiol* 27(7):1480–1482
28. Zhao M, Liu Z, Sha Y et al (2016) Readout-segmented echo-planar imaging in the evaluation of sinonasal lesions: a comprehensive comparison of image quality in single-shot echo-planar imaging. *Magn Reson Imaging* 34(2):166–172. <https://doi.org/10.1016/j.mri.2015.10.010>
29. Yu JY, Zhang D, Huang XL et al (2020) Quantitative Analysis of DCE-MRI and RESOLVE-DWI for differentiating nasopharyngeal carcinoma from nasopharyngeal lymphoid hyperplasia. *J Med Syst* 44(4):75. <https://doi.org/10.1007/s10916-020-01549-y>
30. Mathur A, Jain N, Kesavadas C et al (2015) Imaging of skull base pathologies: role of advanced magnetic resonance imaging techniques. *Neuroradiol J* 28(4):426–437. <https://doi.org/10.1177/1971400915609341>
31. Lee JH, Seo JH, Park KH et al (2012) A case of malignant small round cell tumor of temporal bone with facial paralysis. *Korean J Audiol* 16(3):145–147. <https://doi.org/10.7874/kja.2012.16.3.145>

Publisher's Note Springer Nature remains neutral with regard to jurisdictional claims in published maps and institutional affiliations.